Available online at www.sciencedirect.com
SCIENCE DIRECT®
Journal of Power Sources 149 (2005) 1–7
JOURNAL OF POWER SOURCES
www.elsevier.com/locate/jpowsour

Preparation and characterization of Pt/C and Pt–Ru/C electrocatalysts for direct ethanol fuel cells

Zhaolin Liu [a,*], Xing Yi Ling [a], Xiaodi Su [a], Jim Yang Lee [a,b], Leong Ming Gan [a]

[a] *Institute of Materials Research and Engineering, 3 Research Link, Singapore 117602, Singapore*
[b] *Department of Chemical and Biomolecular Engineering, National University of Singapore, 10 Kent Ridge Crescent, Singapore 119260, Singapore*

Received 5 December 2004; received in revised form 3 February 2005; accepted 4 February 2005
Available online 20 March 2005

Abstract

Nano-sized Pt and Pt–Ru colloids are prepared by a microwave-assisted polyol process, and transferred to a toluene solution of decanthiol. Vulcan XC-72 is then added to the toluene solution to adsorb the thiolated Pt and Pt–Ru colloids. Transmission electron microscopy examinations show nearly spherical particles and narrow size distributions for both supported and unsupported metals. The carbon-supported Pt and Pt–Ru nanoparticles are activated by thermal treatment to remove the thiol stabilizing shell. All Pt and Pt–Ru catalysts (except Pt_{23}–Ru_{77}) give the X-ray diffraction pattern of a face-centered cubic (fcc) crystal structure, whereas the Pt_{23}–Ru_{77} alloy is more typical of the hexagonal close packed (hcp) structure. The electro-oxidation of liquid ethanol on these catalysts is investigated at room temperature by cyclic voltammetry. The results demonstrate that the alloy catalyst is catalytically more active than pure platinum. Preliminary tests on a single cell of a direct ethanol fuel cell (DEFC) indicate that a Pt_{52}–Ru_{48}/C anode catalyst gives the best electrocatalytic performance among all the carbon-supported Pt and Pt–Ru catalysts.

Keywords: Pt/C and Pt–Ru/C electrocatalysts; Direct ethanol fuel cell; Cyclic voltammetry; Microwave-assisted polyol process

1. Introduction

Carbon-supported Pt or Pt-based alloys are the best electrocatalysts for the anodic and cathodic reactions in fuel cells. It is well known that the catalytic activity of the metal is strongly dependent on the particle shape, size, and size-distribution [1]. Conventional preparation techniques based on wet impregnation and chemical reduction of the metal precursors often do not provide adequate control of particle shape and size [1]. There is continuing effort to develop alternative synthesis methods based on microemulsions [2], sonochemistry [3,4], and microwave irradiation [5–9]; all of which are, in principle, more conducive to generate colloids and clusters on the nanoscale, and with greater uniformity.

Legratiet et al. [10] reported a significant increase in particle size when the metal content in a commercial E-TEK Pt/Vulcan carbon catalyst is increased from 10 to 60 wt.%. The metal particle-size for a 10 wt.% Pt catalyst was 2.0 nm, but increased to 3.2 and 8.8 nm for 30 and 60 wt.% Pt catalyst, respectively. Other studies and patents [11–14] have also underlined the difficulty of using conventional methods to preparing platinum catalysts with high metal loadings (>20 wt.%) and small particle sizes (1–2 nm). In a study by Boennemann et al. [15], organoaluminum-stabilized bimetallic colloids with particle size smaller than 2 nm were prepared and deposited on a commercial support at room temperature. The stabilizing surfactant shell on the metal particles had to be removed before the particles could be used for electrocatalysis. In another method first used by Yu et al. [5] that is generally known as the polyol process, an ethylene glycol solution of the metal salt was refluxed at 393–443 K to generate in situ reducing species from ethylene glycol for the reduction of the metallic species. Conductive heating is often used, but microwave dielectric loss heating may be a better synthesis option in view of its energy efficiency, speed, uniformity and

* Corresponding author. Tel.: +65 6872 7532; fax: +65 6872 0785.
E-mail address: zl-liu@imre.a-star.edu.sg (Z. Liu).

0378-7753/$ – see front matter © 2005 Elsevier B.V. All rights reserved.
doi:10.1016/j.jpowsour.2005.02.009

simplicity in execution [16]. Wang and Hsing [17] prepared Pt and Pt–Ru/C catalysts based on an alcohol-reduction process. The surfactant-protected Pt/C and Pt–Ru/C catalysts were prepared using H_2PtCl_6, $RuCl_3$, dodecyldimethyl(3-sulfo-propyl)ammonium hydroxide, carbon black in a mixture of methanol and water to form a suspension, which was refluxed, filtered and washed. In comparison with commercial E-TEK electrocatalysts of similar compositions, the Pt/C catalyst showed similar performance for oxygen reduction and the Pt–Ru/C for oxidation of H_2/CO mixtures. We have proposed a new method of preparing carbon-supported Pt and Pt–Ru catalysts that are active at room temperature for the electro-oxidation of methanol [18,19], as part of our continuing work on the development of low-cost processes for the preparation of homogenous and well-defined nanoparticle catalysts for fuel-cell applications.

In the present work, thiol-encapsulated Pt and Pt–Ru colloids are synthesized by a microwave-assisted polyol process, deposited on carbon, and then heat-treated to produce carbon-supported Pt and Pt–Ru catalysts. The electrochemical activities of these catalysts for ethanol oxidation are investigated.

2. Experimental

2.1. Colloid synthesis

Analytical grades of hydrogen hexachloroplatinate hydrate, ruthenium chloride, sodium hydroxide, ethylene glycol, toluene, and decanethiol were used for the synthesis. All aqueous solutions were prepared with distilled de-ionized water.

A 2 ml sample of aqueous 20 mM hydrogen hexachloroplatinate hydrate solution was mixed with 25 ml of ethylene glycol to produce a yellowish solution. The solution was placed in a CEM microwave reactor for 60 s with the maximum temperature set at 170 °C. The solution changed its colour from yellow to yellowish-brown upon heating, and was left to cool to room temperature naturally. The cooled mixture was diluted with 1–2 times its volume of distilled de-ionized water. The diluted Pt colloid solution was added to 25 ml of a toluene solution of decanethiol to provide a thiol/Pt molar ratio in the range of 3–10. The biphasic mixture was vigorously stirred for a few minutes during which the transfer of Pt from the ethylene glycol–water phase to toluene occurred to leave a clear aqueous solution. The synthesis of the binary Pt–Ru nanoparticles was carried out similarly, using $(1.2 - x)$ ml of 20 mM of H_2PtCl_6, x ml of 20 mM $RuCl_3$ and 25 ml of ethylene glycol in the starting mixture. The value of x was chosen to yield initial Pt to Ru mole ratios of 0.25, 1, 2 and 4. The Pt–Ru products were later known as Pt_{20}–Ru_{80}, Pt_{50}–Ru_{50}, Pt_{67}–Ru_{33}, and Pt_{80}–Ru_{20}, respectively, where the numerical subscripts beside Pt and Ru denote the atomic percentage of the respective alloying metal.

To determine the actual platinum and ruthenium contents in the Pt–Ru alloys, inductively coupled plasma spectroscopy (ICP) was used to measure the unreacted metal ions remaining in the ethylene glycol–water mixtures. The Pt–Ru alloy nanoparticles of compositions of Pt_{23}–Ru_{77}, Pt_{52}–Ru_{48}, Pt_{72}–Ru_{28}, and Pt_{85}–Ru_{15} were obtained from precursors of Pt_{20}–Ru_{80}, Pt_{50}–Ru_{50}, Pt_{67}–Ru_{33}, and Pt_{80}–Ru_{20}. The ruthenium contents in the Pt–Ru alloy nanoparticles were conspicuously lower than in the initial mixtures. This is because some Ru^{3+} ions failed to reduce simultaneously with Pt^{4+} ions within 30 s of reaction time as the redox potential of Ru^{3+}/Ru ($E_0 \sim 0.84$ V) is much lower than that of Pt^{4+}/Pt ($E_0 \sim 1.41$ V) [20].

2.2. Preparation of catalysts

The stable thiol-encapsulated Pt and Pt–Ru colloids were supported on high surface-area Vulcan XC-72 carbon (as-synthesized Pt and as-synthesized Pt–Ru colloid catalysts, 20 wt.% metal content) by combining a toluene dispersion of Pt or Pt–Ru colloid with a suspension of Vulcan carbon in toluene. The solution was vigorous stirred for 2 h. The solvent was evaporated and the solid residue was rinsed with ethanol. Finally, the powder was dried at 60 °C in vacuum.

In order to remove the stabilizing shell on the nanoparticles, the as-synthesized Pt and Pt–Ru colloid catalysts were heat-treated in argon for 1–10 h at 360 °C. The furnace was purged with argon gas for at least 15 min prior to the heat treatment. All the catalysts had a nominal metal loading of 20 wt.% on the Vulcan carbon-black support. The heat-treated samples are identified as heat-treated Pt and heat-treated Pt–Ru catalysts in the following discussion.

2.3. Catalyst characterization

The Pt or Pt–Ru colloidal formation process was monitored by UV–vis spectroscopy on a Shimadzu UV-2501 PC double-beam spectrophotometer in the region of 220–800 nm, using quartz cuvettes of 1 cm path length. The particle morphology, size and size-distribution of the colloids and catalysts were characterized by transmission electron microscopy (TEM) using a Philips CM300 FEG system that was operated at 300 kV. The TEM samples were prepared by placing a drop of the colloidal dispersion or a catalyst suspension sonicated for 1 h in acetone on a 3 mm Cu grid, followed by drying at ambient conditions. X-ray diffraction (XRD) patterns were recorded by means of a Bruker GADDS diffractometer with an area detector using a Cu Kα source ($\lambda = 1.54056$ Å) operating at 40 kV and 40 mA. The XRD samples were obtained by depositing carbon-supported nanoparticles on a glass slide and then drying under vacuum overnight.

2.4. Electrochemical measurements

An EG&G Model 273 potentiostat/galvanostat and a conventional three-electrode test cell were used for electrochemical measurements. The working electrode was

a thin layer of Nafion-impregnated catalyst cast on a vitreous carbon disc that was held in a Teflon cylinder. The catalyst layer was obtained as follows: (i) a slurry was first prepared by sonicating for 1 h a mixture of 0.5 ml of de-ionized water, 0.013 g of Pt/C or Pt–Ru/C catalyst and 0.11 g of Nafion solution (Aldrich: 5 wt.% Nafion); (ii) 1 μl of the slurry was pipetted and spread on the carbon disc; (iii) the electrode was dried at 90 °C for 1 h and mounted on a stainless-steel support. The surface-area of the vitreous carbon disc was 0.25 cm^2. Platinum gauze and a saturated calomel electrode (SCE) were used as the counter and the reference electrode, respectively. All potentials are reported with respect to the SCE. Each electrolyte solution was de-aerated with high-purity argon for 2 h prior to measurement. For cyclic voltammetry experiments, the electrolyte solution was 2 M C_2H_5OH in 1 M H_2SO_4, which was prepared from high-purity sulfuric acid, high-purity grade methanol, and distilled water.

The MEA (membrane electrode assembly) for a direct ethanol fuel cell (DEFC) was made by hot-pressing pretreated Nafion® 117 together with an anode sheet and a cathode sheet. The anode sheet was a carbon paper (SGL, Germany) with a carbon-supported Pt or Pt–Ru catalyst layer. The cathode sheet was a carbon paper with a carbon-supported 40 wt.% Pt catalyst layer supplied by E-TEK. The average platinum loadings at the anode and cathode were 3 and 2 mg cm^{-2}, respectively, and the effective electrode area was 6 cm^2. The fuel was 2 M C_2H_5OH delivered at 2 ml min^{-1} by a micropump, and the oxygen flow was regulated by a flowmeter at 500 cm^3 min^{-1}.

3. Results and discussion

The formation of Pt colloids via microwave dielectric heating was followed by UV–vis spectroscopy. The H_2PtCl_6 solution before microwave irradiation is pale yellow, and shows a peak at 260 nm in its UV–vis spectrum (Fig. 1) as a result of the ligand-to-metal charge-transfer transition in the $PtCl_6^{2-}$ ion [21,22]. The solution turns dark brown after the reaction and the peak at 260 nm is no longer visible, which suggests that all the $PtCl_6^{2-}$ ions are completely reduced. The spectrum of the completely reduced solution displays strong absorption from 700 nm and gradually increases intensity from the visible to the ultraviolet region. These features confirm the formation of colloids [23]. When the Pt colloid in ethylene glycol is diluted with distilled de-ionized water, and mixed with a toluene solution of decanethiol, transfer of Pt from the ethylene glycol and water phase to toluene takes place. This is visually evident from the colour change in the two phases. The colour of the ethylene glycol and water solution fades gradually to colourless, whereas the colour of the toluene and hexane phase darkens from colourless to yellowish-brown or dark brown.

Addition of NaOH to $RuCl_3$ (or a mixture of H_2PtCl_6 and $RuCl_3$) causes an instant colour change from dark brown to yellow-green, due to the formation of ruthenium hydroxide

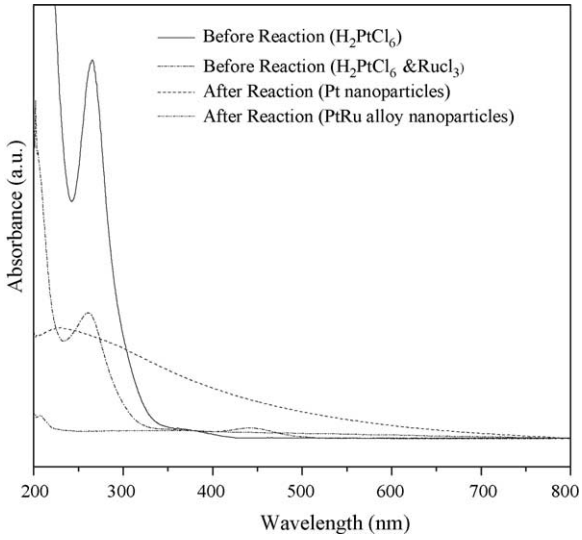

Fig. 1. UV–vis absorption spectra of solution containing H_2PtCl_6, and mixture of H_2PtCl_6 and $RuCl_3$ before and after microwave irradiation.

complexes. This is also shown spectroscopically as the evolution of a peak at ~436 nm. The observation is similar to that of Pârvulescu et al. [24]. On the formation of Pt–Ru alloy nanoparticles, the characteristic absorptions by Ru^{3+} and $PtCl_6^{2-}$ ions at 436 and 260 nm disappear and are replaced by gradually decreasing absorption from the ultraviolet region to 700 nm. This indicates the formation of Pt–Ru nanoparticles.

Typical TEM images of the Pt and Pt_{52}–Ru_{48} colloids, presented in Fig. 2(a) and (b), respectively, show remarkably uniform and high dispersion of the metal and the alloy particles. The average diameters of 4.7 nm (for Pt) and 4.5 nm (for Pt_{52}–Ru_{48}) are accompanied by relatively narrow particle-size distributions (Fig. 2(e) and (f), range: 3–6 nm, standard deviation = 0.4 nm). Adsorption of the colloidal particles on Vulcan carbon followed by thermal treatment (in an argon gas at 360 °C for 5 h) to remove the stabilizing alkanethiol layer do not bring about any significant morphological changes (Fig. 2(c) and (d)). The Pt and alloy nanoparticles are in a state of high dispersion over the carbon surface, and the size of the particles is nearly unchanged.

The XRD pattern of as-synthesized Pt/C under different heat-treatment conditions is given in Fig. 3. The strong diffraction at $2\theta < 35^\circ$ is not shown because it pertains mostly to the carbon-black support. The peaks can be indexed to the [1 1 1], [2 0 0], [3 1 1], [2 2 2] reflections of a Pt face-centered cubic (fcc) crystal structure. The lattice constant of 3.924 Å (for all Pt/C catalysts) is in good agreement with 3.923 Å for pure Pt.

The as-prepared Pt/C displays considerable crystallinity before the heat treatment. As expected the degree of crystallization increases with the heating time, as shown by the sharper and more intense diffraction peaks. The heat treatment produces mostly improvements in crystallinity.

X-ray diffraction patterns are also collected for Pt–Ru alloy nanoparticles supported on carbon black. Generally Ru

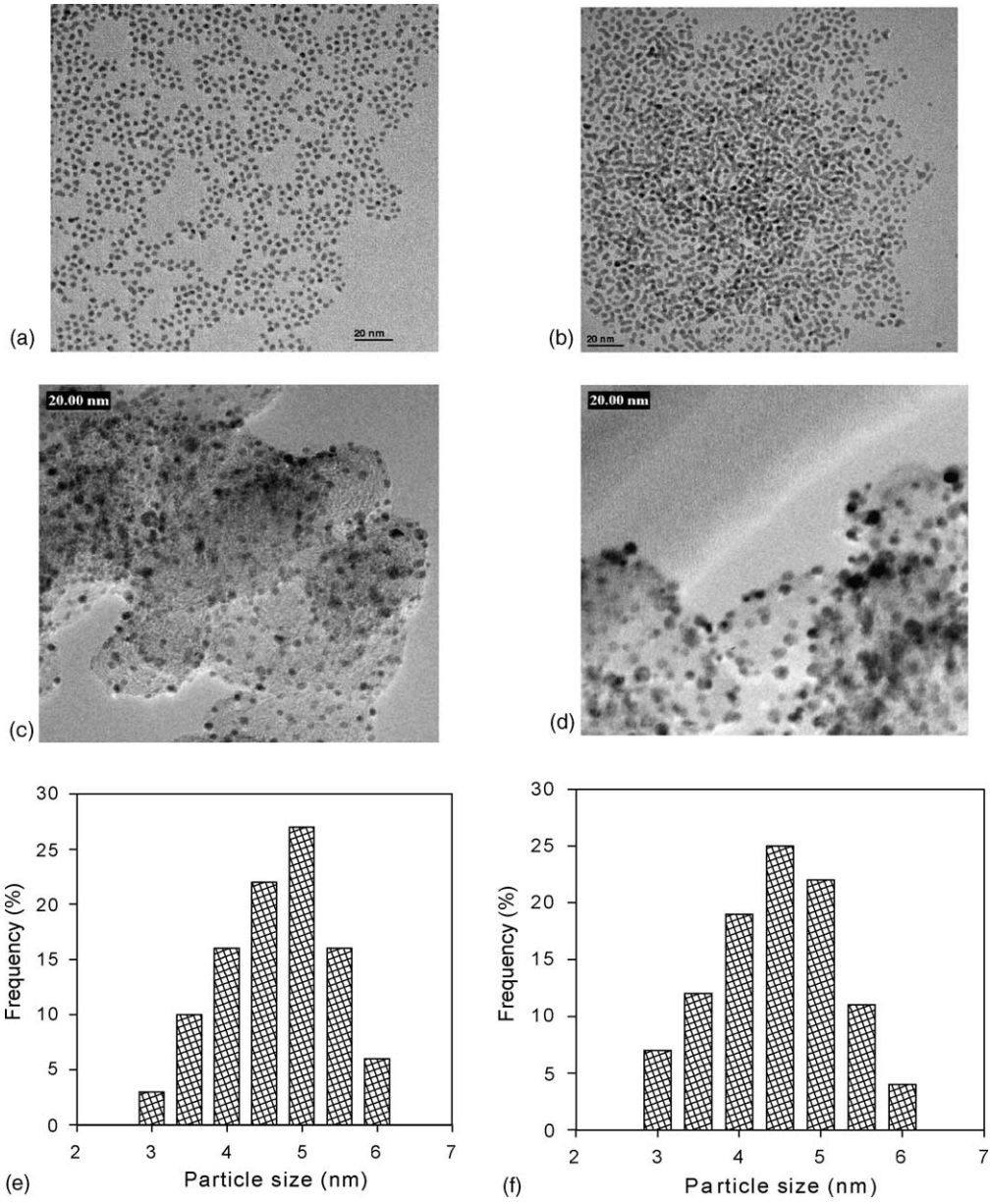

Fig. 2. TEM images of as-synthesized: (a) Pt and (b) Pt–Ru colloid catalysts and (c) heat-treated Pt and (d) Pt–Ru catalysts. Histograms of particle-size distributions for (e) as-synthesized Pt and (f) Pt–Ru colloids.

alone would display the [1 0 0], [1 0 1], [1 1 0], [1 0 3], [2 0 1] reflections of a hcp lattice, whereas Pt would display the characteristic fcc reflections described previously. As seen from the data in Fig. 4, the diffraction pattern of heat-treated Pt–Ru/C (except for Pt_{23}–Ru_{77}) displays mostly the reflection characteristics of the Pt fcc structure, which suggests an alloy formation based on the substitution of the Pt lattice sites [25]. The Pt_{23}–Ru_{77} alloy nanoparticles are exceptional, for which a hcp pattern can be clearly identified and indicates the presence of Ru-rich alloys [26]. It is noted that with increasing proportion of Ru in the Pt–Ru alloys, all (except for Pt_{23}–Ru_{77}) diffraction peaks are shifted synchronously to higher 2θ values. The shift is an indication of the reduction in lattice constant.

The Pt/C and Pt_{52}–Ru_{48}/C catalysts are characterized by cyclic voltammetry (−0.2–1 V, 50 mV s^{-1}) in an electrolyte of 1 M H_2SO_4 and 2 M ethanol, and the resulting voltammograms are shown in Fig. 5. The forward scan oxidation peak of ethanol on both Pt/C and Pt_{52}–Ru_{48}/C appears at about 0.75 V. The current density on the forward scan peak of ethanol electro-oxidation on Pt_{52}–Ru_{48}/C is higher than that on Pt/C. In the reverse scan, an anodic peak current density is detected at around 0.5 V for Pt/C and 0.4 V for Pt_{52}–Ru_{48}/C. Iwasita and Pastor [27] reported that the adsorbed residues of ethanol (e.g., Pt–OCH_2CH_3, Pt–CHOH–CH_3, $(Pt)_2$=COH–CH_3, Pt–$COCH_3$, and Pt=C=O) are difficult to oxidize at low potentials. Thus, they constitute a catalyst poison. Manohara

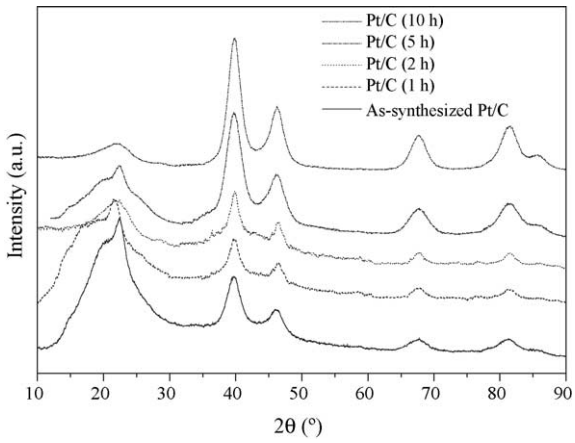

Fig. 3. X-ray diffraction patterns of as-synthesized and various heat-treated Pt/C catalysts.

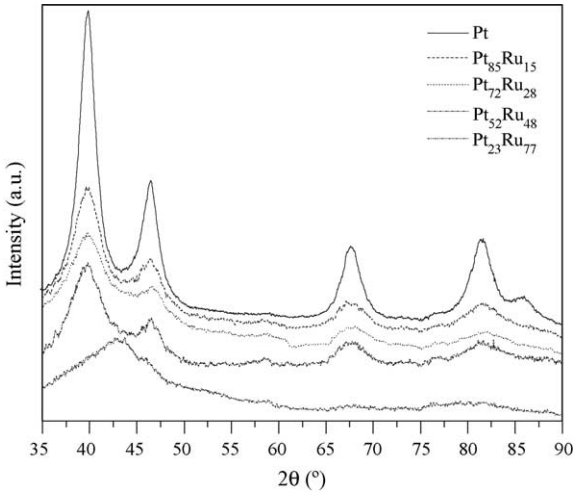

Fig. 4. X-ray diffraction patterns, from top to bottom: heat-treated Pt/C, Pt_{85}–Ru_{15}/C, Pt_{72}–Ru_{28}/C, Pt_{52}–Ru_{48}/C and Pt_{23}–Ru_{77}/C.

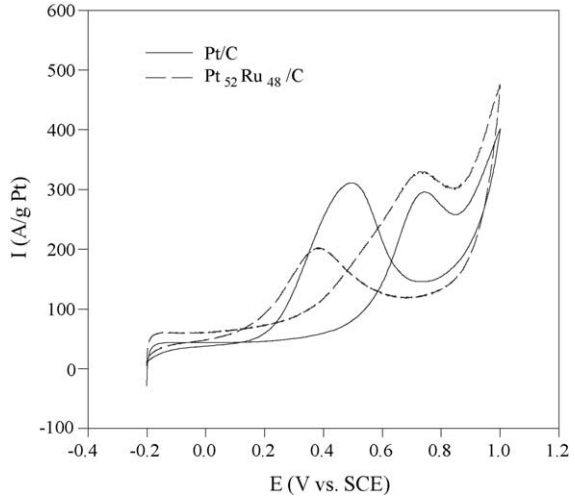

Fig. 5. Cyclic voltammograms of Pt/C and Pt_{52}–Ru_{48}/C catalysts in 1 M H_2SO_4, 2 M ethanol electrolyte.

and Goodenough [28] attributed this anodic peak in the reverse scan to the removal of the incompletely oxidized carbonaceous species formed in the forward scan in an electrolyte. Hence, the ratio of the forward anodic peak current density (I_f) to the reverse anodic peak current density (I_b), I_f/I_b, can be used to describe the tolerance of the catalyst to the accumulation of carbonaceous species. A low I_f/I_b ratio indicates poor oxidation of alcohol to carbon dioxide during the anodic scan, and excessive accumulation of carbonaceous residues on the catalyst surface. A high I_f/I_b ratio shows the converse case. From the results given in Fig. 5, the ratio is 0.96 for Pt/C and 1.60 for Pt_{52}–Ru_{48}/C. Such a low value for the Pt/C indicates that a large amount of intermediate carbonaceous species is not oxidized to carbon dioxide in the forward scan. These experimental observations highlight the major deficiency of pure Pt catalysts, i.e., the accumulation of intermediate carbonaceous species on the catalyst surface that leads to catalyst poisoning.

Cyclic voltammograms for ethanol oxidation on Pt/C and Pt_{52}–Ru_{48}/C catalysts with different forward potential scan limits are shown in Fig. 6. It has been reported [29] that the reaction mechanism of ethanol oxidation on Pt electrodes in acid medium involves parallel and consecutive oxidation reactions, as follows:

$$CH_3{-}CH_2OH \rightarrow CH_3{-}CHO + 2H^+ + 2e^- \quad (1)$$

$$Pt + CH_3{-}CHO \rightarrow Pt{-}(CO{-}CH_3)_{ads} + H^+ + e^- \quad (1')$$

$$Pt + Pt{-}(CO{-}CH_3)_{ads} \rightarrow Pt{-}(CO)_{ads} + Pt{-}(CH_3)_{ads} \quad (1'')$$

$$CH_3{-}CH_2OH + H_2O \rightarrow CH_3{-}COOH + 4H^+ + 4e^- \quad (2)$$

Reaction (1) occurs mainly at lower potentials ($E < 0.6$ V versus reversible hydrogen electrode (RHE)) and reaction (2) occurs mainly at higher electrode potentials ($E > 0.8$ V versus RHE). At intermediate potentials (0.6 V versus RHE $< E <$ 0.8 V versus RHE), the dissociative adsorption of water occurs:

$$Pt + H_2O \rightarrow Pt{-}OH_{ads} + H^+ + e^- \quad (3)$$

so that the oxidation of adsorbed CH_3–CHO may produce acetic acid, as follows:

$$(CH_3{-}CHO)_{ads} + Pt{-}OH_{ads} \rightarrow (CH_3{-}COOH)_{ads} + H^+ + e^- + Pt \quad (4)$$

Further oxidation to carbon dioxide is usually difficult on pure Pt electrodes at room temperature. Carbon monoxide acting as a poisoning species, and CO_2 have been clearly observed by infrared reflectance spectroscopy [30] and gas chromatography [31]. This may be explained by reactions (1′), (1″) and (5):

$$Pt{-}(CO)_{ads} + Pt{-}OH_{ads} \rightarrow 2Pt + CO_2 + H^+ + e^- \quad (5)$$

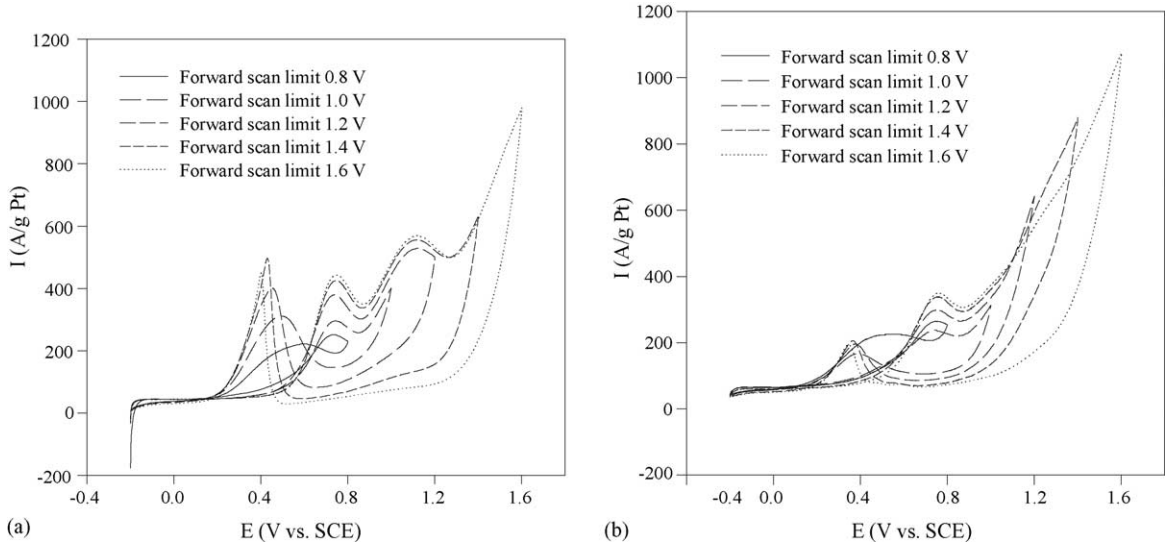

Fig. 6. Cyclic voltammograms of room temperature ethanol oxidation on (a) Pt/C and (b) Pt_{52}–Ru_{48}/C catalysts in 1 M H_2SO_4, 2 M C_2H_5OH at 50 mV s^{-1} with different forward potential scan limits.

Since the backward scan peak current for the Pt/C catalyst increases with increase of the anodic limit of the forward scan (Fig. 6(a)), it appears that the backward scan peak is associated with freshly chemisorbed species (such as CH_3–COOH and Pt–$(CO)_{ads}$). The backward scan peak current for the Pt_{52}–Ru_{48}/C catalyst decreases with increase in the anodic limit on the forward scan (Fig. 6(b)), it appears that the existence of Ru facilitates the oxidation of freshly chemisorbed species and displays an enhanced activity for ethanol electrooxidation. The reaction of the backward scan peak may be explained by:

$$\text{Pt–Ru–OH}_{ad} + \text{Pt–Ru=C=O} \rightarrow 2\text{Pt–Ru} + \text{CO}_2 + \text{H}^+ + \text{e}^- \quad (6)$$

$$2\text{Pt–Ru–OH}_{ad} + (\text{CH}_3\text{–COOH})_{ads} \rightarrow 2\text{Pt–Ru} + 2\text{CO}_2 + 6\text{H}^+ + 6\text{e}^- \quad (7)$$

Hence, the I_f/I_b ratio increases with the anodic limit.

The performance of single cells with different Pt–Ru/C samples as anode catalysts is given in Fig. 7. As identified in the cyclic voltammetry test, Pt_{52}–Ru_{48}/C shows a higher activity than that of Pt/C and the other Pt/Ru mole ratio catalysts. The open-circuit voltage of the single fuel cell using different Pt–Ru/C catalysts cannot be distinguished see Fig. 7(a). The performance and power density of the single fuel cell increases with the Ru content in the Pt–Ru/C catalysts, and the best cell performance and the highest power density appear when Pt_{52}–Ru_{48}/C is employed as the anode

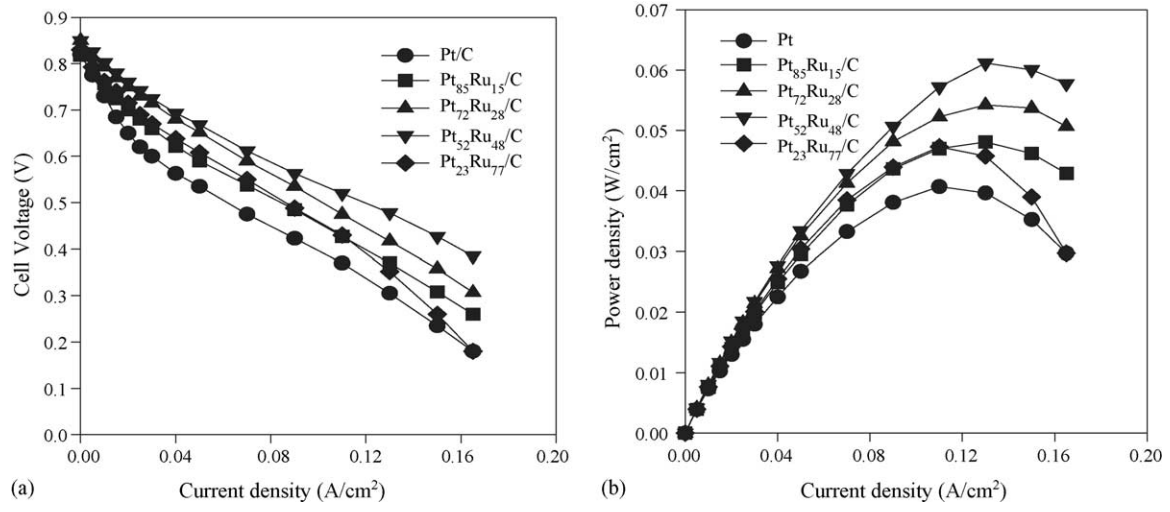

Fig. 7. Polarization curves and output power of single cell at operating temperature of 80 °C. Anode: Pt–Ru/C with different Pt/Ru mole ratio (3 mg cm^{-2}), 2 M C_2H_5OH 2 ml min^{-1}. Cathode: Pt/C (E-TEK) (2 mg cm^{-2}), O_2 1 bar.

catalyst. When the mole percent of ruthenium is increased to 77%, i.e., Pt_{23}–Ru_{77}/C, the performance and power density decreases. Nevertheless, Pt–Ru/C is better as an anode catalyst than Pt/C.

4. Conclusions

Pt and Pt–Ru nanoparticles supported on Vulcan XC-72 carbon are prepared by the microwave-assisted polyol process. In this process, Pt and Pt–Ru colloids are first formed in an ethylene glycol solution and subsequently transferred to toluene using decanethiol as the phase-transfer agent. The metal particles are nano-sized (4.7 nm for Pt, and 4.5 nm for Pt–Ru) and have relatively narrow particle-size distributions (range: 3–6 nm, standard deviation ∼0.4 nm). X-ray diffraction analysis shows that the as-synthesized Pt already has considerably crystallinity that is further refined by heat treatment. All the Pt–Ru/C catalysts (except Pt_{23}–Ru_{77}) display the characteristic diffraction peaks of the Pt fcc structure, but the 2θ values are all shifted to slightly higher values. The metal colloids are adsorbed on Vulcan XC-72 carbon and heat-treated to remove the decanethiol shell. The resulting catalysts are active at an operating temperature of 80 °C for the electro-oxidation of ethanol, especially in the case of Pt_{52}–Ru_{48}. The binary catalyst is more active than the Pt-only catalyst.

References

[1] I.S. Armadi, Z.L. Wang, T.C. Green, A. Henglein, M.A. El-Sayed, Science 272 (1996) 1924.
[2] Z.L. Liu, J.Y. Lee, M. Han, W.X. Chen, L.M. Gan, J. Mater. Chem. 12 (2002) 2453.
[3] K. Okitsu, A. Yue, S. Tanabe, H. Matsumoto, Chem. Mater. 12 (2000) 3006.
[4] T. Fujimoto, S. Teraushi, H. Umehara, I. Kojima, W. Henderson, Chem. Mater. 13 (2001) 1057.
[5] W.Y. Yu, W.X. Tu, H.F. Liu, Langmuir 15 (1999) 6.
[6] W.X. Tu, H.F. Liu, Chem. Mater. 12 (2000) 564.
[7] S. Komarneni, D.S. Li, B. Newalkar, H. Katsuki, A.S. Bhalla, Langmuir 18 (2002) 5959.
[8] W.X. Chen, J.Y. Lee, Z.L. Liu, Chem. Commun. (2002) 2588.
[9] Z.L. Liu, J.Y. Lee, W.X. Chen, M. Han, L.M. Gan, Langmuir 20 (2004) 181.
[10] B. Legratiet, H. Remita, G. Picq, M.O. Delcourt, J. Catal. 164 (1996) 36.
[11] A. Gamez, D. Richard, P. Gallezot, F. Gloaguen, R. Faure, R. Durand, Electrochim. Acta 41 (1996) 307.
[12] M. Watanabe, K. Sakairi, US Patent 5,728,485 (1998).
[13] K. Tsurumi, P. Stonehart, US Patent 5,480,851 (1995).
[14] P. Stonehart, US Patent 5,593,934 (1997).
[15] H. Boennemann, R. Binkmann, P. Britz, U. Endruschat, R. Moertel, U.A. Paulus, G.J. Feldmeyer, T.J. Schmidt, H.A. Gasteiger, R.J. Behm, J. New Mater. Electrochem. Syst. 3 (2000) 199.
[16] S.A. Galema, Chem. Soc. Rev. 26 (1997) 233.
[17] X. Wang, I-M. Hsing, Electrochim. Acta 47 (2002) 2981.
[18] Z.L. Liu, X.Y. Ling, J.Y. Lee, X.D. Su, L.M. Gan, J. Mater. Chem. 13 (2003) 3049.
[19] Z.L. Liu, X.Y. Ling, X.D. Su, J.Y. Lee, J. Phys. Chem. B 108 (2004) 8234.
[20] F.A. Cotton, G. Wildinson, Advanced Inorganic Chemistry, Wiley, 1988.
[21] T. Teranishi, M. Hosoe, T. Tanaka, M. Miyake, J. Phys. Chem. B 103 (1999) 3818.
[22] S.Y. Zhao, S.H. Chen, S.Y. Wang, D.G. Li, H.Y. Ma, Langmuir 18 (2002) 3315.
[23] D.N. Furlong, A. Launikonis, W.H.F. Sesse, L.V. Sanders, J. Chem. Soc., Faraday Trans. 1 80 (1984) 571.
[24] V.I. Pârvulescu, S. Coman, P. Palade, D. Macovei, C.M. Teodorescu, G. Filoti, R. Molina, G. Poncelet, F.E. Wagner, Appl. Surf. Sci. 141 (1999) 164.
[25] E. Antolini, L. Giorgi, F. Cardellini, E. Passalacqua, J. Solid State Electrochem. 5 (2001) 131.
[26] D. Chu, S. Gilman, J. Electrochem. Soc. 143 (1996) 1685.
[27] T. Iwasita, E. Pastor, Electrochim. Acta 39 (1994) 531.
[28] R. Manohara, J.B. Goodenough, J. Mater. Chem. 2 (1992) 875.
[29] C. Lamy, E.M. Belgsir, J.M. Léger, J. Appl. Electrochem. 31 (2001) 799.
[30] J.M. Pérez, B. Beden, F. Hahn, A. Aldaz, C. Lamy, J. Electroanal. Chem. 262 (1989) 251.
[31] H. Hitmi, E.M. Belgsir, J.M. Léger, C. Lamy, R.O. Lezna, Electrochim. Acta 39 (1994) 407.